forests

MDPI

Article

Improving Individual Tree Crown Delineation and Attributes Estimation of Tropical Forests Using Airborne LiDAR Data

Wan Shafrina Wan Mohd Jaafar [1,2,*], Iain Hector Woodhouse [1], Carlos Alberto Silva [3,4], Hamdan Omar [5], Khairul Nizam Abdul Maulud [2,6], Andrew Thomas Hudak [7], Carine Klauberg [8], Adrián Cardil [9] and Midhun Mohan [10,11]

1 School of Geosciences, University of Edinburgh, Edinburgh EH8 9XL, UK; i.h.woodhouse@ed.ac.uk
2 Earth Observation Centre, Institute of Climate Change (IPI), Universiti Kebangsaan Malaysia, Bangi 43600, Malaysia; knam@ukm.edu.my
3 Biosciences Laboratory, NASA Goddard Space Flight Center, Greenbelt, MD 20707, USA; carlos_engflorestal@outlook.com
4 Department of Geographical Sciences, University of Maryland, College Park, Maryland, MD 20740, USA
5 Forest Research Institute Malaysia, Kepong 52109 FRIM, Malaysia; hamdanomar@frim.gov.my
6 Smart & Sustainable Township Research Center, Faculty of Engineering and Built Environment, Universiti Kebangsaan Malaysia, Bangi 43600, Malaysia
7 USDA Forest Service, Rocky Mountain Research Station, 1221 South Main Street, Moscow, ID 83843, USA; ahudak@fs.fed.us
8 Federal University of São João Del Rei—UFSJ, Sete Lagoas 35701-970, MG, Brazil; carine_klauberg@hotmail.com
9 Tecnosylva, Parque Tecnológico de León, 24009 León, Spain; adriancardil@gmail.com
10 Department of Forestry and Environmental Resources, North Carolina State University, 2800 Faucette Drive, Raleigh, NC 27695, USA; mmohan2@ncsu.edu
11 Department of Operations Research, North Carolina State University, 2310 Stinson Drive, Raleigh, NC 27695, USA
* Correspondence: wanshafrina@gmail.com or wanshafrina@ukm.edu.my

Received: 9 August 2018; Accepted: 29 November 2018; Published: 5 December 2018

Abstract: Individual tree crown (ITC) segmentation is an approach to isolate individual tree from the background vegetation and delineate precisely the crown boundaries for forest management and inventory purposes. ITC detection and delineation have been commonly generated from canopy height model (CHM) derived from light detection and ranging (LiDAR) data. Existing ITC segmentation methods, however, are limited in their efficiency for characterizing closed canopies, especially in tropical forests, due to the overlapping structure and irregular shape of tree crowns. Furthermore, the potential of 3-dimensional (3D) LiDAR data is not fully realized by existing CHM-based methods. Thus, the aim of this study was to develop an efficient framework for ITC segmentation in tropical forests using LiDAR-derived CHM and 3D point cloud data in order to accurately estimate tree attributes such as the tree height, mean crown width and aboveground biomass (AGB). The proposed framework entails five major steps: (1) automatically identifying dominant tree crowns by implementing semi-variogram statistics and morphological analysis; (2) generating initial tree segments using a watershed algorithm based on mathematical morphology; (3) identifying "problematic" segments based on predetermined set of rules; (4) tuning the problematic segments using a modified distance-based algorithm (DBA); and (5) segmenting and counting the number of individual trees based on the 3D LiDAR point clouds within each of the identified segment. This approach was developed in a way such that the 3D LiDAR points were only examined on problematic segments identified for further evaluations. 209 reference trees with diameter at breast height (DBH) $\geq$ 10 cm were selected in the field in two study areas in order to validate ITC detection and delineation results of the proposed framework. We computed tree crown metrics

(e.g., maximum crown height and mean crown width) to estimate aboveground biomass (AGB) at tree level using previously published allometric equations. Accuracy assessment was performed to calculate percentage of correctly detected trees, omission and commission errors. Our method correctly identified individual tree crowns with detection accuracy exceeding 80 percent at both forest sites. Also, our results showed high agreement ($R^2 > 0.64$) in terms of AGB estimates using 3D LiDAR metrics and variables measured in the field, for both sites. The findings from our study demonstrate the efficacy of the proposed framework in delineating tree crowns, even in high canopy density areas such as tropical rainforests, where, usually the traditional algorithms are limited in their performances. Moreover, the high tree delineation accuracy in the two study areas emphasizes the potential robustness and transferability of our approach to other densely forested areas across the globe.

Keywords: tropical forest; individual tree crown (ITC); LiDAR; 3D LiDAR point cloud; canopy height model (CHM); mathematical morphology; watershed; aboveground biomass (AGB)

1. Introduction

Individual tree information is important in many forestry-related activities, such as biodiversity assessment, selective cuts, silviculture treatment, and tree growth modelling [1]. Advances in remote sensing techniques and products, especially in light detection and ranging (LiDAR) technologies, have improved the feasibility of individual tree-based analyses. In the past decade, airborne LiDAR has become the leading remote sensing technology for characterizing 3D forest structure, as LiDAR data enable the extraction of canopy and crown structure attributes at varying spatial resolutions to provide a more meaningful structural description of forests. Individual tree crown detection and delineation (ITC) is an approach that has been used in many useful forestry studies to estimate AGB [2,3], identify species [4], and analyse gaps in the forests [5].

The utility of ITC delineation has promoted the development of various methods using airborne LiDAR data [6–11]. A comprehensive overview of LiDAR applications for ITC detection and delineation is contained in [12]. Most of these methods are based on raster-based approaches, utilising LiDAR-derived canopy height models (CHM) [13–16]. In a typical CHM-oriented procedure, treetops are first detected using local maxima or a similar filtering approach before delineating the individual tree crowns with a marker-controlled watershed segmentation or pouring algorithm scheme [16–20]. However, in closed canopy conditions, tree crowns and tree branches have similar shapes and overlap each other, and current individual tree crown delineation methods work less effectively [6].

For methods based on CHM-oriented tree crown delineations, the CHM is typically smoothed to constrain the number of tree tops detected via local maximum filtering using a fixed or variable-sized window [21]. However, the allometric relationship between tree height and crown width can sometimes be weak, especially in closed canopies such as a tropical primary forest [22]. Thus, it is difficult to determine an optimal filter size for the local maximum filtering to retain the multi-scale crowns. CHM-oriented tree crown delineations have been focused on both single scale and multi-scale analyses, although multi-scale analysis techniques have been proposed and developed to overcome this issue [23] since trees naturally vary in age, size, and crown morphology, and this approach provides a more robust solution for tree crown delineation [24,25].

Multi-scale ITC delineation can be achieved using several techniques or strategies. One approach uses 2D wavelets of varying size to filter the CHM images and detect tree crowns at multiple scales [26]. Reference [27] evaluated the usefulness of Laplacian and Gaussian filters to segment digital surface model (DSM) images, and subsequently applied a marker-controlled watershed segmentation method to subdivide the filtered image resulting from multiple segmentation maps. It is also possible to detect tree crowns based on the correlation between the CHM and a series of 3D crown models [28]. All these methods are based on the 3D geometric shapes of multi-scale tree crowns. However, the scales used were set manually or iteratively through trial-and-error. While successful and useful, these methods

typically produce higher omission and commission errors, especially in mixed wood, closed canopy, and deciduous forests [29].

With the advancement of LiDAR systems of increased point density, newer approaches directly utilize the 3D LiDAR point clouds for ITC segmentation. Cluster-based methods, especially K-means clustering, are some of the most recent and popular approaches to directly extract individual trees from the original LiDAR data. Here, n observations are partitioned into k clusters, where each observation is grouped into a cluster according to the nearest mean value by minimising the overall sum of Euclidean distances of the points from the cluster centroids in feature space [30,31]. Also, an adaptive clustering method was developed by [32] to delineate individual trees using LiDAR data in a managed pine forest. Nonetheless, this method required a copious amount of training data to perform supervised learning. On the other hand, reference [33] sequentially segmented individual trees, from the tallest to the shortest, by adopting a top-to-bottom region growing approach. Additionally, mean shift-based clustering techniques have also been applied to LiDAR data to delineate individual trees [34–38]. The main drawback of these methods, which work directly with 3D LiDAR point clouds, is that they are computationally heavy and require high-performance computers to process huge amounts of data, as opposed to using derived rasters.

The aim of this study was to develop an efficient framework for ITC segmentation to improve the accuracy and efficiency of ITC delineation from LiDAR data by using the well-established CHM-based methods, the more detailed 3D point cloud characterization of tree crowns, and field reference data. Finally, this data allowed the estimation of individual tree attributes such as AGB, height and crown width.

2. Material and Methods

2.1. Study Area Description

The Pasoh Forest Reserve (PFR) and the Forest Research Institute Malaysia (FRIM) Forest Reserve in Peninsular Malaysia were selected as the study areas because of their closed forest canopies, tree species and structural diversity [39,40]. The PFR study site is located 8 km from Simpang Pertang, Negeri Sembilan and the FRIM site is located at Kepong, Selangor, approximately 16 km northwest of the capital city of Kuala Lumpur and 140 km away from PFR (Figure 1). Both study areas featured lowland dipterocarp forests of similar structures. Also, since these areas were stripped of their original forest cover and logged over 100 years ago, the present secondary forests are almost as old as the primary forests. Further details about the study sites can be found in [10].

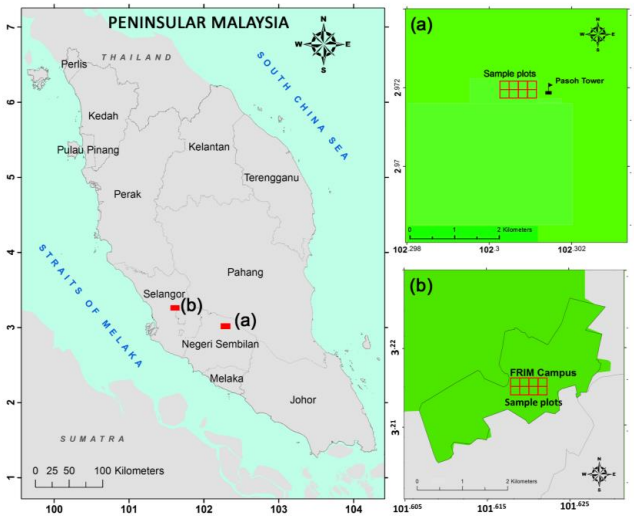

Figure 1. Location of the study area (Peninsular Malaysia) and sample plots; (**a**) Pasoh Forest Reserve (PFR) plot and, (**b**) Forest Research Institute Malaysia (FRIM) plot. The size of each rectangular plot was 0.5 ha (50 m × 100 m) and was subdivided into eight experimental subplots (25 m × 25 m). Adapted from [10].

2.2. Field Data Collection

As a part of the data collection procedure, we used a rectangular plot of side length 50 m × 100 m, which was subdivided into eight experimental subplots, each with dimensions of 25 m × 25 m [10], to examine and assess our methodology. From these plots, a total of 105 reference trees at PFR and 104 reference trees at FRIM with a diameter at breast height (DBH) ≥ 10 cm were selected and measured (Table 1). There were five main forest parameters collected at tree level during the field campaign: horizontal position (x, y) of individual trees, DBH, total height, crown diameter, and tree species. The tree positions were recorded using a Trimble Laser Ace 1000 rangefinder with a precision of 50 cm after post-processing. The plot centres were geolocated using a total station. Tree stem positions were recorded relative to plot center locations, which were post-processed with local base station data, resulting in an average error of approximately 50 cm horizontally. Tree heights were measured using a hypsometer, and the DBH and crown diameter were measured using a diameter tape (d-tape). To measure the crown diameter, the point on the ground which was exactly below the branch tip on one end of the measurement was first located and marked. Afterwards, on moving to the opposite side of the crown, we located the point under the corresponding branch tip. Here, the spread along the line gives the horizontal distance between two positions, which equals the crown diameter; the crown radius was measured in orthogonal directions with respect to the tree trunk. To measure crown sides which were not easily accessible, such as with the case of trees growing on cliff sides or steep angles, a laser range-finder was used. The AGB (kg tree^{-1}) was obtained through previous allometric models calibrated for the study sites [10]. The AGB model had adjusted coefficients of determination (adj-R^2) of 0.63 and an absolute root mean squared error (RMSE) of 14.8% kg tree^{-1} [10].

Table 1. Characteristics of individual tree field sample data from both forest sites, mean ± SD (n).

Tree Attributes	Sites	
	PFR	FRIM
Tree height (m)	18.16 ± 6.87	33.42 ± 9.17
DBH (cm)	29.33 ± 19.15	37.92 ± 20.86
Crown diameter (m)	4.14 ± 2.18	7.35 ± 3.26
AGB (kg)	918.74 ± 1562.55	2421.80 ± 2162.92
Number of trees (n)	105	104

Note: Only trees with a DBH ≥ 10 cm were measured and considered in this table; SD = Standard deviation. DBH: diameter at breast height; ABG: aboveground biomass.

2.3. LiDAR Data Acquisition and Data Processing

LiDAR data for the PFR site were obtained with a Riegl Q560 sensor using an IGI LiteMapper-5600 system (IGI, Kreuztal, Germany) scanning at a ±22.5° scan angle with an average point density of 8.8 points per m^2 and a vertical accuracy of ±15 cm RMSE. LiDAR data for the FRIM site were obtained with an ALTM Gemini laser system scanning at ±25° with an average point density of 7.5 points per m^2 and a vertical accuracy of ±15 cm RMSE. FUSION/LDV software (Version 3.80) [41] was used to process the LiDAR data to generate three main products: the digital terrain model (DTM), the digital surface model (DSM) and the canopy height model (CHM). The CHM was generated by differencing the DSM and the DTM, as shown for the PFR and FRIM sites in Figure 2. The 1-m resolution CHM was generated using the *CanopyModel* function of FUSION software [41]. For effective elimination of noise, the CHM was smoothed with a 3 × 3 Gaussian low pass filter, as per the technique presented in [31]. Further details on the LiDAR data and processing workflow can be found in [10].

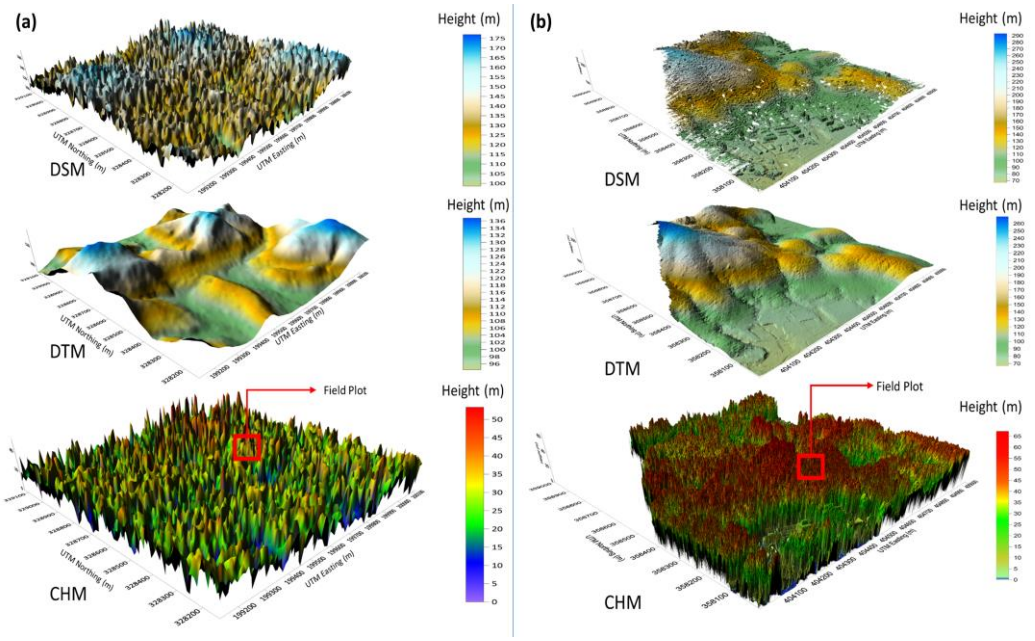

Figure 2. Derivation of the canopy height models (CHMs) as the difference between the digital surface model (DSM) and digital terrain model (DTM) for (**a**) PFR site and (**b**) FRIM site.

2.4. Individual Tree Crown (ITC) Delineation

The framework developed to improve the accuracy of ITC delineation consisted of five steps (Figure 3): (1) determining the dominant crown size from the CHM images through an automatic procedure that employs semi-variogram statistics and morphological analysis; (2) producing the opening tree segments from the CHM image based on the determined crown size using a watershed algorithm based on mathematical morphology; (3) identifying the opening tree segments and evaluating the problematic segments for refinement by a set of rules determined prior to exploring the study sites; (4) refining the pre-determined segments which were marked as problematic by using the modified distance-based algorithm (DBA) developed by [33]; and (5) tallying the identified trees based on the 3D LiDAR points in each of the pre-determined segments.

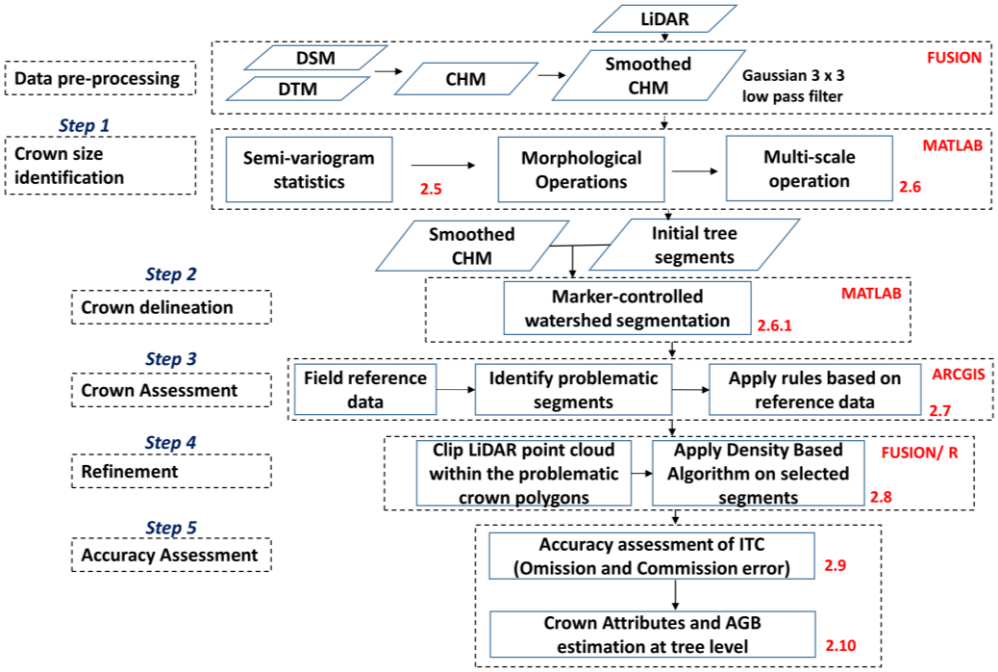

Figure 3. Flowchart of the individual tree crown (ITC) delineation methodology. LiDAR: light detection and ranging.

2.5. Crown Structure Characterisation (Step 1)

Characterizing spatial structures—based on their sizes and shapes—through morphological opening operations can separate different types of objects within a grayscale image. Herein, applying the aforementioned principle, various tree crowns within a LiDAR-derived CHM were set apart. Structuring elements (SE), a feature of the morphological analysis process, successfully isolated objects of different sizes [42]. SE can be viewed as a matrix consisting of either 0s (erosion) or 1s (dilation) with respect to different sizes and shapes. Objects that completely covered the SE were reserved and truncated, while others were eliminated. By applying this to the CHM, opening operations with disk SEs could separate different sizes of tree crowns. Here, the 3D shape of a tree crown was considered to be a half ellipsoid (Figure 4); these half ellipsoids described the crown structures as either fine or coarse. If the tree crown was sliced from top to bottom into many layers (Figure 4a1–c1), a disk was fitted to each of the resulting slices from top to bottom. The height values decreased continuously from the treetop to the lower crown boundary. By looking at the 3D perspective, the CHM image was vertically scanned with the algorithm along a horizontal plane from top to bottom. The sizes of the half ellipsoids (hence, the size of the tree crown) were determined from the largest disk diameter at the bottom of each slice. As a result, the size of the tree crown could be estimated using mathematical morphology with a disk structuring element (SE) [42]. This process is graphically illustrated in Figure 4. As can be noted from the figures, Tree B (the taller tree) produced an earlier cross-section (Figure 4a2) compared to tree A (the shorter tree). As the disk SE scans down, the cross-sections are expanded with the decrease in scanning heights (Figure 4b2,c2). This cross-section process is a continuous step (tree A and tree B), where tree cross sections that appear in a previous step must be contained in the following cross-section. Cross-sections of individual tree crown regions that do not connect with others typically appear circular (Figure 4a2,b2), and cross-sections produced by overlapping trees often appear as an irregular shape (Figure 4c2).

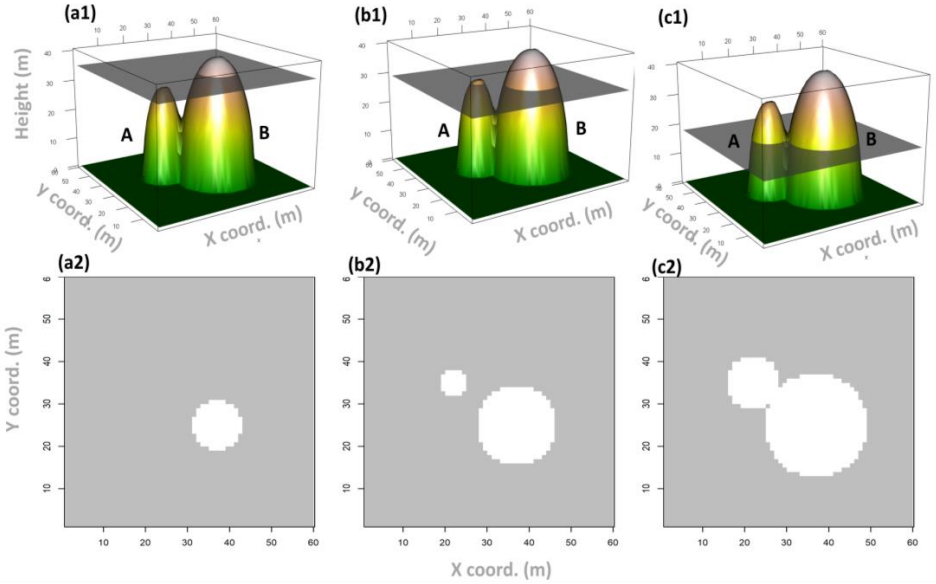

Figure 4. Graphical illustration of separating different sized tree crowns using the disk structuring elements (SE)-based process on a CHM, containing tree A (smaller) and tree B (larger). The illustrations (**a1**–**c1**) represent the scanning window process on CHM, and (**a2**–**c2**) are the corresponding cross-sections produced from (**a1**) to (**c1**), respectively.

To investigate the potential sizes of tree crowns, a series of disk SEs with diameters of 1–19 pixels were used in the morphological opening operation on a CHM image to generate a series of opened CHM images. These opened CHM images are marked as OC_i, i = 1, 3, . . . , 19, where i is the diameter of the SE used to generate OC_i. For the continuous opened images, OC_i and OC_{i+2}, where i and i+2 indicate the corresponding SE diameters, the mean value and their difference (OC_{i+2}–OC_i) were generated. If there are any significant differences in object sizes between two adjoining opened images, a local minimum will occur. From the assessed CHM, mean values indicated the dominant sizes and the range of sizes of objects. The object's size ranges at the PFR and FRIM sites were large and comprised multiple dominant sized groups. For this study, 1 pixel was considered equivalent to 1 m and the windows ranged in sizes of 1–2 pixels, 3–5 pixels, 7–11 pixels, 13–15 pixels and 17–19 pixels. The sizes of branches were marked in the first object group, while the four other groups were categorized as small, medium, or large tree crowns, or tree clusters. To indicate the group range, the minimum value of each tree crown size was treated to be the group representative for the three dominant tree crown sizes; 1, 3 and 7 pixels marked the group representative of the PFR site and 3, 7 and 13 pixels marked the group representative of the FRIM site. These hereafter will be referred to as small, medium, or large tree crown levels.

Considering the high stem density and closed canopy structure of forests in the study area, further analysis was required for the satisfactory delineation of tree crowns of different sizes. Semi-variogram statistics were used to estimate the range of crown sizes within the CHM [42] as their ability to characterise the spatial structures of observed surface properties have been demonstrated in previous studies [43,44]. A semi-variogram works by measuring half the variance between pairs of pixels at increasing separation (lag) distances, thus indicating the spatial scale of variability in the observed canopy height. At zero separation distance (lag = 0), the semi-variogram value is zero. The semi-variance increases with lag distance until it reaches a plateau at a lag distance from which the first derivative can be used to infer the maximum crown size. Tree crowns at both sites were grouped as small, medium, or large based on being 1–2 pixels, 3–5 pixels and 7–11 pixels at the PFR site, and 3–5 pixels, 7–11 pixels and 13–15 pixels at the FRIM site. Since the tree crown level was selected based on the minimum value within the crown group size, objects with a larger size were retained for filtering or for a morphological opening operation.

2.6. Multi-Scale Operations (Step 2)

The principal of the multi-scale operation procedure was to identify the tree tops for marker-controlled watershed segmentation. The algorithm assumed (i) a tree crown in a CHM can be considered as a half-ellipsoid that represents the fine or coarse structures, and (ii) the horizontal extent at a certain height can be determined through the crown horizontal cross-section which contains its tree tops at a specific height. Afterwards, a morphological opening operation with a disk SE of diameter d was applied to the CHM to remove tree crowns that were smaller than the disk SE while truncating the others horizontally. The tree tops of the truncated crowns were similar to the horizontal cross-sections at certain heights. Trees varied in size and some branches had a size similar to individual trees in the forest. Multiple opening operations (e.g., multiple layers of cross-sections) with different sized SE disks were required to sort all of the tree crowns and to merge different layers of cross-sections together to generate a tree crown markers layer.

Another underlying assumption was that a tree crown in a CHM usually appears as a circle, whereas a tree cluster, as a combination of several crowns, is less circular [25]. The circularity (c) threshold of a segment [27] was calculated as

$$c = Acluster / Acircle \quad (1)$$

where *Acluster* is the area of the crown cluster and *Acircle* is the area of the crown radius. The multiple layers were consolidated to retain only unique tree crowns as follows:

1. Cross-sections with a circularity less than a threshold of 0.85 [27] were removed to eliminate tree clusters;
2. To merge cross-sections of layers, the logic "OR" operation was used;
3. The merged cross-sections were refined by removing those with any circularity less than the threshold.

The cross-section results showed the positions of the tree crowns, which were then used as a marker for watershed segmentation.

Marker-Controlled Watershed Segmentation

In this study, the commonly used marker-controlled watershed segmentation was used to separate the CHMs at different scales [45,46]. This raw CHM was then smoothed using a Gaussian filter. The filtering kernel of the Gaussian filter is detailed as follows:

$$g(x, y, \sigma) = \frac{1}{2\pi\sigma} e^{-(\frac{x^2+y^2}{2\sigma^2})} \quad (2)$$

where x and y were the distance to the centre of the smoothing kernel. σ was used to adjust the parameters of the Gaussian function, and a 3 × 3 filtering kernel was used (Figure 5).

g (-1,1, σ)	g(0,1,σ)	g(1,1,σ)
g(-1,0,σ)	g(0,0,σ)	g(1,0,σ)
g(-1,-1,σ)	g(0,-1,σ)	g(1,-1,σ)

Figure 5. A 3 × 3 filtering kernel of a Gaussian smoothing algorithm.

The CHM was smoothed by moving the aforementioned kernel filter. For the pixel $p(X, Y)$ located in the nucleus of the filtering kernel, DN value was computed as

$$p(X, Y) = \sum_{i=-\frac{d}{2}+1.0}^{\frac{d}{2}-1.0} \sum_{j=-\frac{d}{2}+1.0}^{\frac{d}{2}-1.0} p(X+i, Y+j) \times g(x+i, y+j, \sigma) \quad (3)$$

where X and Y were coordinates of the pixel in the image, d (tree crown size of d pixels) was the size of the filtering template, which was an odd number (i.e., 3, 5, 7 . . .), and i and j were distances to the studied pixel. The filtering template was designed to deal with various 3D radiometric shapes of tree crowns; this has been found to work effectively in a number of previously performed ITC delineation studies [21,26,47,48]. The application of Gaussian filter to a greyscale image—in our case, the CHMs—allowed tree crowns with a similar size and shape to be enhanced and smaller objects to suppressed. Since the tree crown level was the minimum value within a tree crown size group, objects with larger sizes were retained. The three previously determined crown levels led to three Gaussian filters, and thus three filtered CHMs, each containing objects of a similar size and shape.

The marker-controlled watershed segmentation is a multi-step process, with the initial step being the determination of markers indicating the local maxima detected in the CHM at each given scale. Following that, the watershed simulates the immersion from markers to determine the flooded basins—that is, tree crowns in our case. After the initial multi-step process, watershed segmentation was performed across the entire landscape area (100 ha) for both forest sites using marker-controlled watershed segmentation functions available in Matlab (version R2016a; MathWorks, Natick, MA, USA). After the removal of non-crown areas such as buildings and bushes or grass (marked as anything less than two meters, which were previously delineated by a threshold method on the CHM), segmentation maps at multiple scale levels were generated for both forest sites (Figures 6 and 7). Segments with a mean height $\leq$ 2m were considered as gaps and were not analysed further. Tree attributes of tree height, crown width (CW) and AGB were estimated for each single tree across the landscape area.

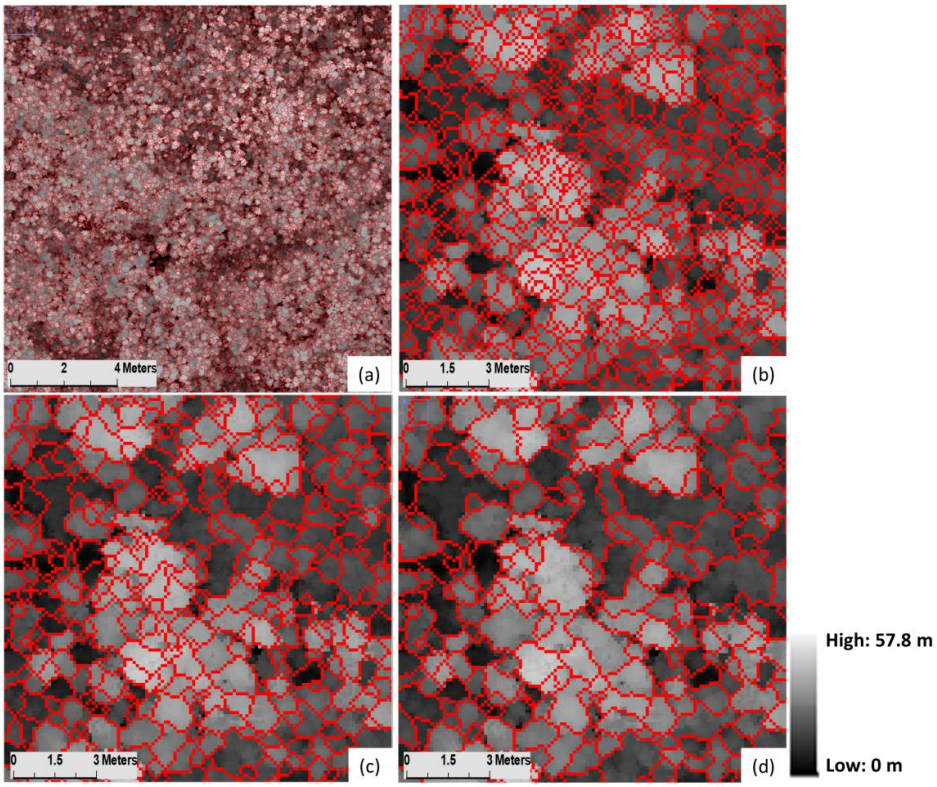

Figure 6. The crown segmentation map of the PFR site: (**a**) crown segmentation map over 100 ha and the segmentation at (**b**) small, (**c**) medium and (**d**) large tree crown levels with the corresponding filtered images in the background.

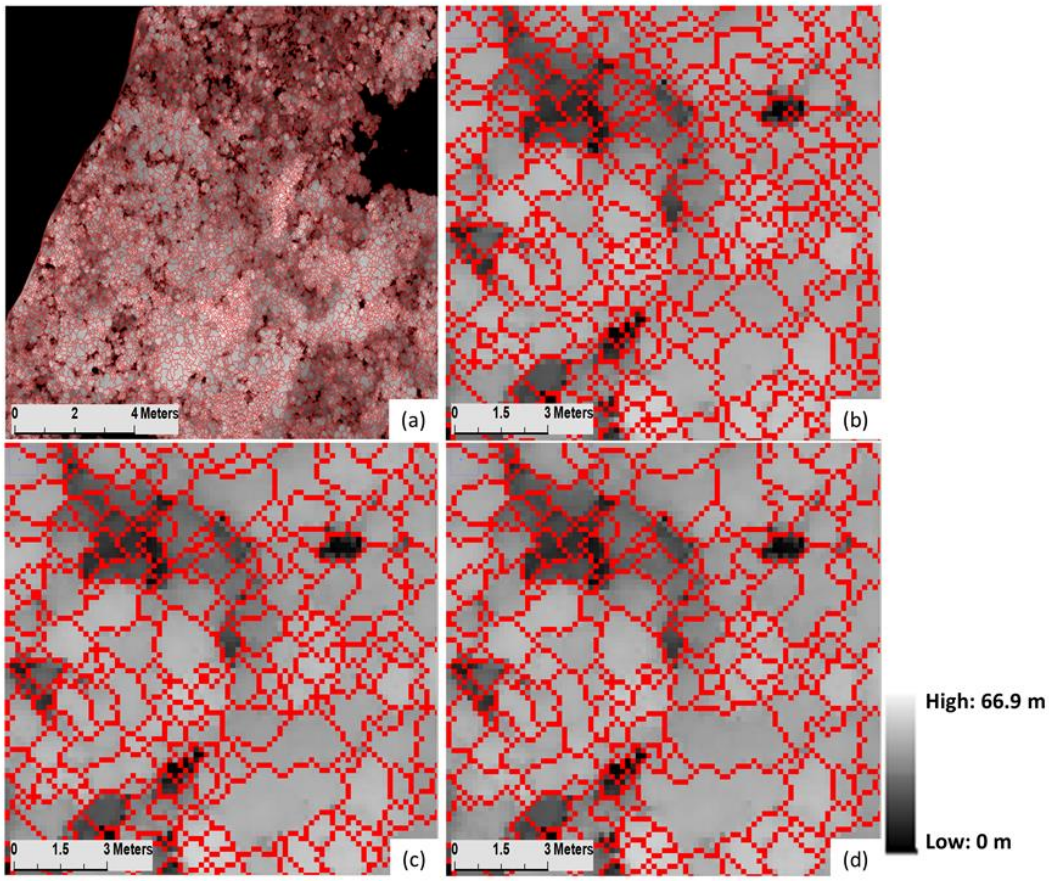

Figure 7. The crown segmentation map of the FRIM site: (**a**) crown segmentation map over 100 ha and the segmentation at (**b**) small, (**c**) medium and (**d**) large tree crown levels with the corresponding filtered images in the background.

2.7. Identification of Problematic Tree Segments (Step 3)

Since there existed the possibility that some watersheds might still represent clusters of trees, a pair of rules were set based on the detected crown size and comparisons with the reference trees, and other crown segment-related information acquired through fieldwork. This increased the accuracy of the identified tree positions and separated neighbouring trees that had contributed a cluster. This additional evaluation process was conducted as exemplified in Figure 8. Segment (*i*) contained two trees, which could not be separated by the watershed segmentation, even though two reference trees were known to exist; here, a second segmentation was run on trees identified as needing segmentation again. The rules that were employed for identifying segments for further refinement are listed below:

- Trees with a crown size greater than 11 m for the PFR site and trees with a crown size greater than 17 m for the FRIM site were identified as not a single tree but as a group of trees. Hence, these trees needed to be segmented again because the largest crown size detected was 10.3 m at the PFR site and 16 m at the FRIM site;
- For identifying potential tree clusters, (i) we set the circularity threshold to 0.85 initially and detected the large segments, then (ii) we flagged the circularity of a small segment as large and the circularity of a large segment as small, and (iii) when a large segment with a low circularity index was classified, it most likely belonged to a tree cluster.

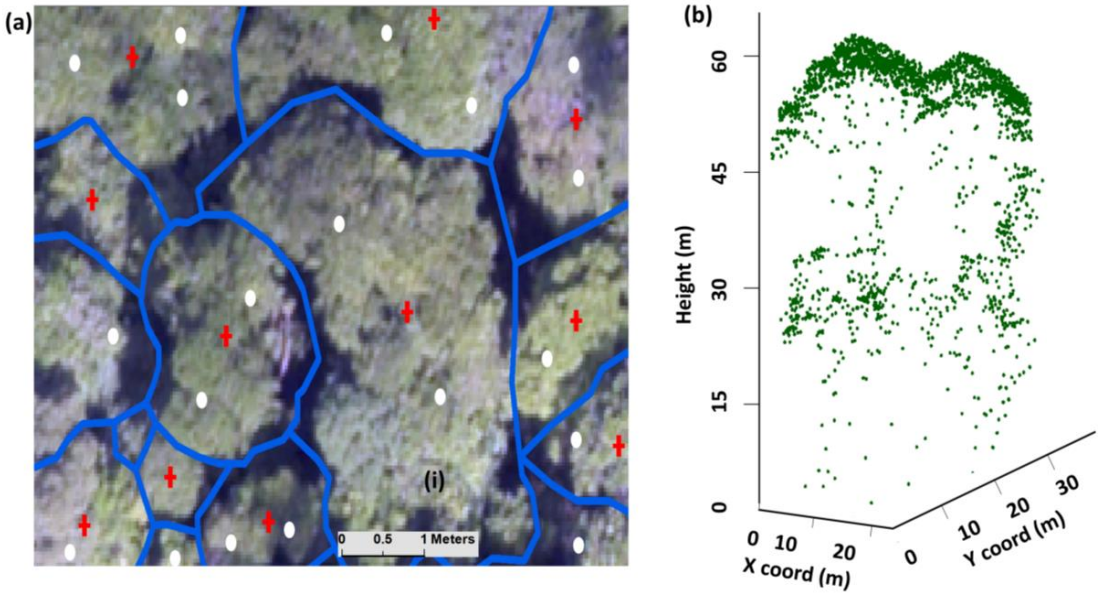

Figure 8. (**a**) Orthophoto with watershed segments (blue), a field reference tree (white) and local maxima (red cross), and (**b**) LiDAR point cloud for the *i* segment.

2.8. Refinement of the Final Tree Crown Delineation Using a Distance-Based Algorithm (DBA) (Step 4)

The refinement of the final tree crown delineation, for the identified problematic segments—which represented more than one tree or no tree—was performed using a distance-based algorithm (DBA) [33] in the lidR package of R [49]. This algorithm isolated each tree individually and sequentially from the point cloud by adopting a top-to-bottom approach to classify the points from the tallest to the shortest tree. If more than one tree was identified (e.g., *n* trees) in a given segment, the DBA worked to separate the *n* tree points in this segment. To identify and group the points into a single tree, the DBA exploits the spacing among the tops of trees. The major uncertainty for tree segmentation in this algorithm was mainly derived from the spacing threshold. A higher threshold can result in under-segmentation, whereas a smaller threshold can result in over-segmentations. For this step, we used an adaptive threshold (dt) to improve the segmentation accuracy: dt was taken to be 1.5 and 1.0 m when tree heights were $\geq$15 and <15 m, respectively. This spacing threshold was chosen based on our knowledge of the forest study areas, plus incorporation of the crown rules as discussed in Section 2.7. It was assumed that the tree spacing at the upper level is >1 m and that the taller trees have larger crown sizes, resulting in larger spacing. Nonetheless, the minimum spacing rule was not used in our case, as it did not improve classification accuracy.

2.9. Accuracy of ITC (Step 5)

The accuracy of the segmentation results was quantified by comparing each detected tree with the nearest reference trees in the 16 test subplots (eight subplots per forest site). The numbers of trees detected per subplot from LiDAR were manually compared with field-based data and evaluated using measures of perfect segmentation, under-segmentation, and over-segmentation which were expressed in terms of true positive (TP), false negative (FN'), or false positive (FP), respectively [33]. If a tree was correctly segmented, it is called TP; if a tree was not detected and assigned to a nearby tree, it is called FN'; if a tree does not exist but is segmented from the point cloud, it is called FP. We evaluated the detection accuracy in terms of "recall", which indicated the tree detection rate, while "precision" indicated the correctness of detected trees and the F-score gives a measure of the overall accuracy. The recall, precision and F-score were formulated as follows [50,51]:

$$\text{recall} = \frac{\text{TP}}{\text{TP} + \text{FN}'} \quad (4)$$

$$\text{precision} = \frac{\text{TP}}{\text{TP} + \text{FP}} \tag{5}$$

$$\text{F} - \text{score} = 2 \times \frac{r \times p}{r + p} \tag{6}$$

Recall was inversely related to omission error and precision was inversely related to commission error. Commission and omission errors were used to represent the calculated means of recall and precision; recall, precision, and F-score values ranged from 0 to 1. In short, a higher F-score indicated a higher r and p value; i.e., lower commission and omission errors [33]. If all trees were correctly segmented, then the r and p values were both equal to one, which resulted in F being equal to one.

2.10. Crown Attribute Assessment and Aboveground Biomass Estimation at Tree Level

To test for improved accuracy, we compared the ITC delineation results with the watershed segmentation output after refinement, using the Wilcoxon–Mann–Whitney rank-sum test statistic [52] at $\alpha = 0.05$. Afterwards, we estimated the aboveground biomass (AGB) using the AGB model developed in [10] for the study site (see Equation (7)) along with tree height and crown size from the LiDAR point clouds that were computed using the CrownMetrics function available in the rLiDAR package [53], and compared our values with reference data to assess the accuracy of our models; the explanatory power of the LiDAR-based models was evaluated using the coefficient of determination (R^2), absolute and relative root mean square error (RMSE, RMSE%; see Equation (8)) and bias (Bias, Bias%; see Equation (9)) between the LiDAR-derived result and field-derived result, computed for a single response variable. The reference data for ITC, tree height and crown size came from fieldwork done in 2014, two years after the LiDAR data were acquired. This notwithstanding, there were no significant changes in tree size over this short period; therefore, it was feasible to locate and compare the crown parameters with the LiDAR data.

$$\text{AGB}_{\text{LiDAR}} = EXP(0.57 + 0.61 \times \text{lnCW} + 1.55\ln h80) \tag{7}$$

where CW is the crown width and $h80$ is the 80th percentile derived from the LiDAR points.

$$\text{RMSE} = \sqrt{\frac{\sum_{i=1}^{n}(L_i - F_i)^2}{n}} \tag{8}$$

$$\text{Bias} = \frac{1}{n}\sum_{i=1}^{n}(L_i - F_i) \tag{9}$$

where L is the LiDAR-derived variable, F is the field-derived variable, and n is the number of reference observations. The relative RMSE and Bias are computed by dividing the absolute RMSE and Bias by the mean of the variable computed over the reference observations and multiplied by 100.

3. Results

3.1. Evaluation of Morphological Watershed Segmentation

Morphological opening operations are important to determine the dominant crown sizes through geometric and structural knowledge of tree crowns. The minimum crown sizes were indicated by the first "clear break" of the semi-variance first derivatives (Figure 9) and, based on these results, crown sizes were classified into four groups. The smallest sizes of each group were denoted as 1, 3 and 7 pixels for the PFR site and 3, 7 and 13 pixels for the FRIM site used in the watershed segmentation process. The cross-sections marked as the opening of the disk size and SE were used as the markers in the marker-controlled watershed segmentation to generate the tree segments. Through visual inspection, it became evident that even though most of the crowns were accurately segmented, when segment boundaries were laid over the original CHM images, a few of them did not match. In these

cases, crown segments were detected as a tree cluster, as this was either visually apparent or known from the reference field data. Based on the criteria discussed in Section 2.7, Figure 10 shows an example of segments in point clouds that needed further refinement relative to results after DBA refinement. Accuracy statistics of the ITC delineation generated using the watershed segmentation with mathematical morphology before and after refinement using DBA for the study sites are listed in Tables 2 and 3.

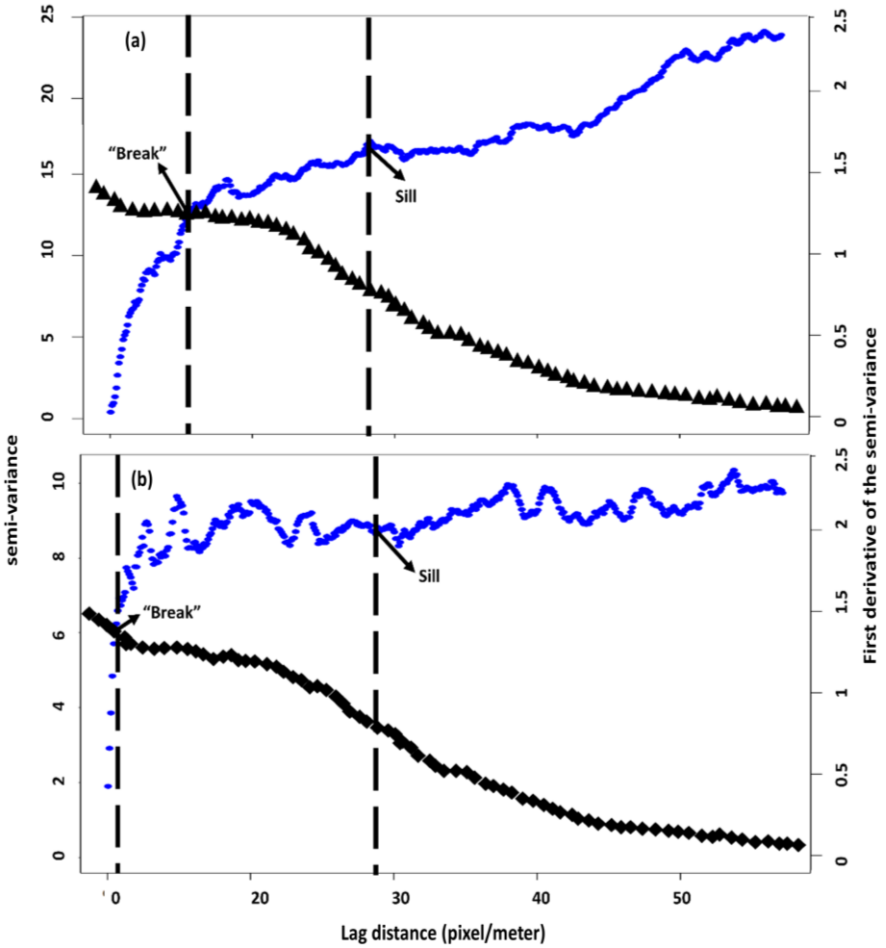

Figure 9. The semi-variogram (blue) of the CHM and its first derivative (black) at the (**a**) PFR site and (**b**) FRIM site. The left vertical dashed line indicates where the break in the slopes of the semi-variogram occurred, and the right vertical dashed line indicates the range where the semi-variogram reached the sill.

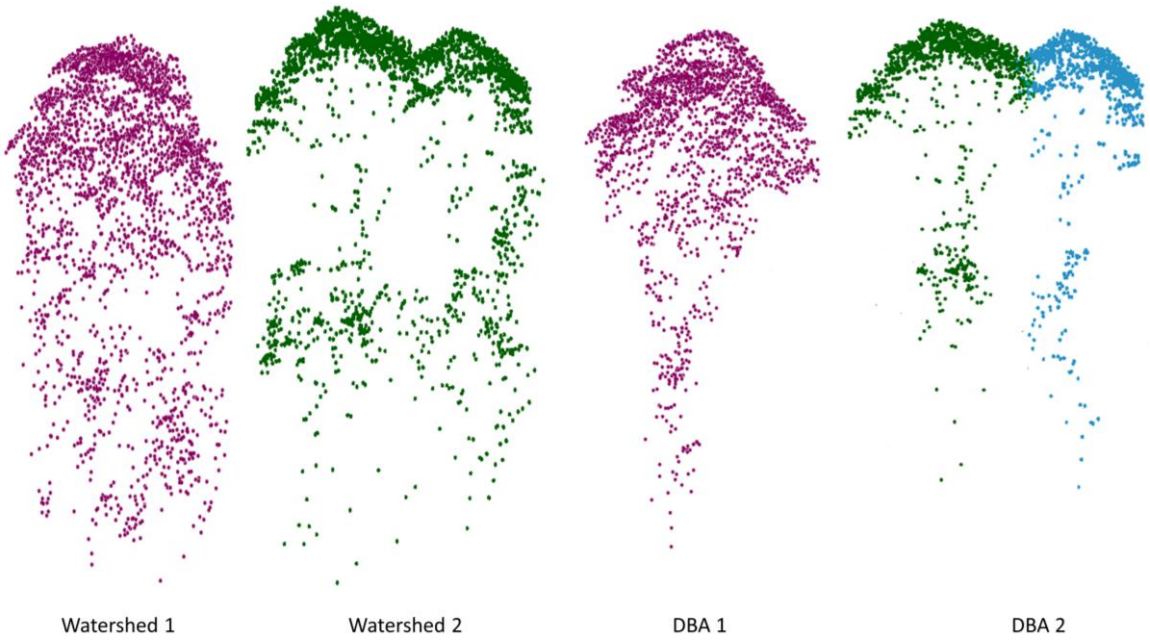

Figure 10. Comparison of watershed delineation results before and after refinement using the DBA. The two trees on the left were segmented using watershed segmentation; the two trees on the right were refined using the DBA. The refinement produced a point cloud that better represented the bole and lower portion of the tree, while the watershed segmentation delineated every point below the surface, including extraneous features that are not part of the tree.

Table 2. Accuracy assessment statistics for tree segmentation using morphological watershed segmentation and the proposed method based on the distance-based algorithm (DBA) at the PFR site.

Method	Subplots	LiDAR	Reference	FP	FN	TP	Recall	Precision	F-Score
Morphological watershed	A1	22	24	2	4	20	0.83	0.91	0.87
	A2	20	23	2	5	18	0.78	0.90	0.84
	A3	26	22	5	3	19	0.86	0.79	0.83
	A4	7	8	1	2	6	0.75	0.86	0.80
	B1	11	4	7	0	4	1.00	0.36	0.53
	B2	7	8	1	2	6	0.75	0.86	0.80
	B3	10	8	4	2	6	0.75	0.60	0.67
	B4	6	8	0	2	6	0.75	1.00	0.86
	Overall	**109**	**105**	**22**	**20**	**85**	**0.81**	**0.79**	**0.80**
Distance-based algorithm	A1	23	24	2	3	21	0.88	0.91	0.89
	A2	22	23	2	3	20	0.87	0.91	0.89
	A3	25	22	5	2	20	0.91	0.80	0.85
	A4	8	8	1	1	7	0.88	0.88	0.88
	B1	6	4	3	1	3	0.75	0.50	0.60
	B2	7	8	1	2	6	0.75	0.86	0.80
	B3	11	8	4	1	7	0.88	0.64	0.74
	B4	4	8	0	4	4	0.50	1.00	0.67
	Overall	**106**	**105**	**18**	**17**	**88**	**0.84**	**0.83**	**0.83**

Note: FP: False positive; FN: False negative; TP: True positive.

3.2. Accuracy Assessment of Tree Detection

To assess the individual tree detection accuracy, we compared the segmented trees with the reference trees in both the forest field sites. Overall, the accuracy of individual tree detection from the watershed segmentation was slightly better at PFR than at FRIM. The segmentation algorithm detected approximately 80.95% of reference trees correctly in the PFR site and 84.6% actual trees in the FRIM site. The associated commission error (false positive) rate and omission error (false negative) rates of the PFR site were 19% and 21% respectively, whereas at the FRIM site, the segmentation resulted in a

commission error rate of 15.4% and an omission error rate of 37.5%. Thus, over-detection outweighed under-detection at both sites (Tables 2 and 3).

In the case of the identified problematic segments, DBA was applied to further refine the crown results. Consequentially, we noticed an improvement in the tree detection results; at the PFR site, we were able to detect 83.8% of reference trees, and at the FRIM site, we detected 88.46% trees correctly. Also, at the PFR site, the segmentation commission error rate decreased from 19% to a 16.2% and the omission error rate decreased from 21% to a 17.14%. Improvements were also observed at the FRIM site, where the commission error rate decreased to 11.53% and omission error rate decreased to 25%. In summary, even though the DBA refinement still showed some over-detection, it slightly improved the results.

Table 3. Accuracy assessment statistics for tree segmentation using morphological watershed segmentation and the proposed method based on the distance-based algorithm (DBA) at the FRIM site.

Method	Subplots	LiDAR	Reference	FP	FN	TP	Recall	Precision	F-Score
Morphological watershed	A1	18	13	6	1	12	0.92	0.67	0.77
	A2	21	17	7	3	14	0.82	0.67	0.74
	A3	20	15	5	0	15	1.00	0.75	0.86
	A4	23	18	7	2	16	0.89	0.70	0.78
	B1	13	11	5	3	8	1.00	0.50	0.67
	B2	14	12	4	2	10	0.83	0.71	0.77
	B3	9	9	3	3	6	0.89	0.38	0.53
	B4	9	9	2	2	7	0.78	0.39	0.52
	Overall	**127**	**104**	**39**	**16**	**88**	**0.85**	**0.69**	**0.76**
Distance-based algorithm	A1	17	13	4	0	13	1.00	0.76	0.87
	A2	21	17	6	2	15	0.88	0.71	0.79
	A3	17	15	3	1	14	0.93	0.82	0.88
	A4	23	18	6	1	17	0.94	0.74	0.83
	B1	12	11	2	1	10	0.91	0.83	0.87
	B2	14	12	3	1	11	0.92	0.79	0.85
	B3	6	9	1	4	5	0.56	0.83	0.67
	B4	8	9	1	2	7	0.78	0.88	0.82
	Overall	**118**	**104**	**26**	**12**	**92**	**0.88**	**0.78**	**0.83**

Note: FP: False positive; FN: False negative; TP: True positive.

3.3. Crown Attributes and AGB Estimates at Tree Level at the Field Plots

The differences of the methodology's performance metrics before and after DBA refinement can be demonstrated through the correlation between the LiDAR-derived result and field-derived results. There was a slightly stronger relationship for the delineation results after DBA refinement compared to the watershed method. The correlation between LiDAR-derived attributes and field reference attributes (Figure 11a2–c2) was also slightly improved after refinement compared to the watershed results (Figure 11a1–c1). Results from the Wilcoxon–Mann–Whitney rank-sum test warranted rejecting the null hypothesis, as evidenced by the p-values ≤ 0.05: 0.04 for tree height, 0.03 for CW, and 0.02 for AGB, meaning there were significant improvement in the results before and after DBA refinement. The distributions of LiDAR-derived and field-derived forest attributes are shown in Figure 11. In general, the correlation between LiDAR-predicted and field-observed attributes were high and the RMSE and Bias were relatively low. Analysing the AGB estimations, Figure 11a1,a2 shows that the error is substantial in the estimation of the large values of AGB. To evaluate further, we assessed the AGB prediction accuracy in terms of quantiles (Table S1). The quantile statistics shows an inverse result, where the relative RMSE and Bias decrease as an increase in quantiles occurs, whereas for large trees, there are fewer RMSE errors in terms of percentage but higher absolute values. Overall, the DBA method showed a better AGB prediction accuracy (RMSE and Bias) compared to the watershed method in quantile 4.

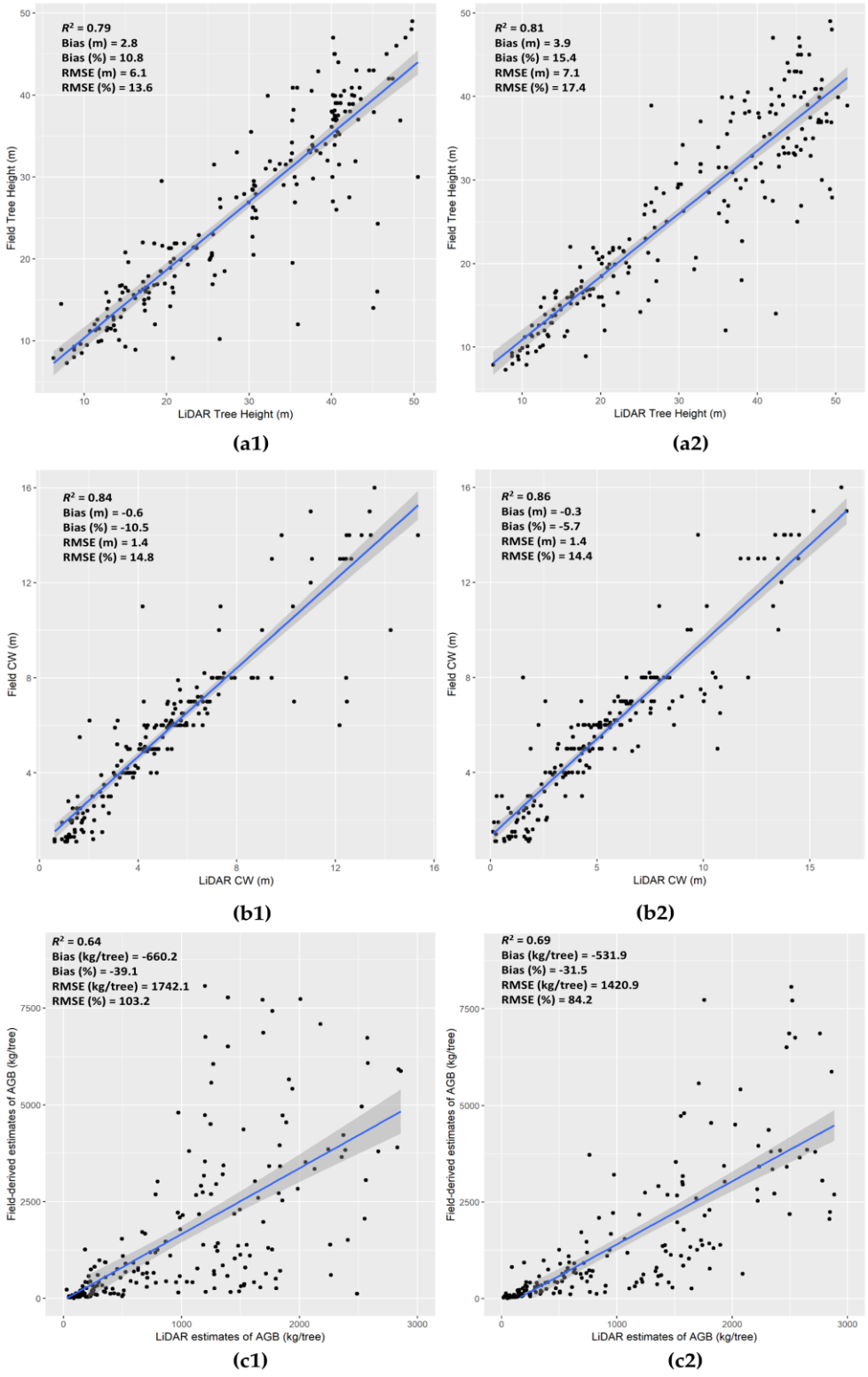

Figure 11. LiDAR-derived tree attributes versus field reference attributes (tree height, crown width (CW), and AGB). (**a1**–**c1**) morphological watershed segmentation results and (**a2**–**c2**) results after refinement with the distance-based algorithm (DBA).

4. Discussion

The usefulness and importance of accurate ITC detection and delineation has promoted the development of different methods and approaches to better characterize the forest structure and

individual tree crowns and attributes [11,12]. Thus, our paper presents a new approach that substantially improves the overall accuracy in the detection of tree crowns by integrating the information on the vertical structure of trees—derived from LiDAR data—with existing ITC delineation strategies. The proposed framework was designed in such a way that a detailed examination of the 3D LiDAR points was performed only on those crown segments that needed further evaluation based on a priori field knowledge, thereby making it time and resource-efficient. The efficacy of our methodology in delineating ITCs was also demonstrated by the satisfactory accuracies obtained with respect to both visual (Figures 6 and 7) and quantitative assessments (Tables 2 and 3). Prior studies reported in the literature [5,19,25] show consistently lower crown delineation accuracies for deciduous forests and tropical forests as compared to conifer forests, due to the fact that deciduous and tropical forests tend to be closely packed, with more irregular crown geometries given that a big tree branch can often resemble a tree crown. Apart from this, several other factors—such as differences in study sites, data used, and evaluation methods—also play a significant role in attaining high accuracies. Nevertheless, the high overall accuracies over two tropical forest sites in this study (80.95% for PFR and 84.6% for FRIM) indicate that our ITC segmentation could generate a map of multi-sized individual tree crowns in forests with accuracies comparable to visual interpretation results. Indeed, our accuracies were higher than those reported in [5,19,25] for deciduous and mixed forests. Studies by [25] as well as [6] employed similar evaluation methods, where both the CHM (in raster format) and the height-normalized LiDAR point clouds were exploited. Here, the ITCs were first defined from the CHM using the multi-scale watershed segmentation method, and later, the LiDAR point clouds were used to reshape the segments; the accuracies for these cases were 65%–73% [25] and 72%–74% [6], respectively. In summary, the delineation results from our studies were about 11%–16% more accurate than the previously mentioned studies. One of the core strengths of our approach is that we validated the ITC delineation result at the tree level using field reference data, which was not the case with several studies that developed methods for delineating ITC from LiDAR point clouds [8].

Our method, based on an efficient framework for ITC segmentation using LiDAR-derived CHM and 3D point cloud data, can improve the accuracy of delineating tree crowns. It is well reported that CHM-based methods produce lower detection accuracy than point-based methods because the former use a raster surface model [6]. For instance, reference [54] documented the performance of ITC by employing object-based analysis (OBIA) to segment the CHM and point cloud segmentation algorithm proposed in [33]; the same algorithm was used in this study to segment the LiDAR data into individual trees. It was reported that OBIA over-segmented many large trees, but in some cases, it correctly delineated smaller trees that the point cloud approach had missed. The point cloud approach also produced larger polygons, especially for the tall and matured trees, but overall both methods detected trees well when compared to the ground reference data, with high coefficients of determination (0.92 and 0.93 respectively). The difference with our study is that the point cloud approach was applied to the 3D LiDAR points clipped with the polygons segmented from the watershed segmentation. Our results were therefore comparable to the results obtained in other studies using both the point cloud and raster-based approaches [54].

Semi-variogram and morphological methods have been used in other studies to improve ITC detection and delineation [23,52,55]. However, in this study, object features were assessed using semi-variogram and morphological methods together with the watershed segmentation algorithm in a coordinated manner. In our case, the crown sizes determined from CHM images of the PFR and FRIM sites were consistent with visual observations. We evaluated the pre-determined segments, generated from the marker-controlled watershed segmentation, by exploiting the geometry of tree crowns bound by a small set of rules. Segments that did not satisfy the rules were identified and evaluated for refinement. If the number of rules applied was sufficient, then the identified problematic segments that needed to be segmented again contained the reference tree information.

The development of new algorithms, techniques and approaches to detect and delineate ITCs using LiDAR data will open new avenues for extending the frontiers of crown delineation and

information extraction from LiDAR data [54,56]. Even though rules for differentiating tree crowns and tree clusters are currently efficient, as with those in our case, several thresholds in the method need to be manually set, and the associated morphological computation is relatively complex, which could be improved in future studies; for instance, more advanced rules could be developed to account for less circular tree crowns. A few studies have explored the possibility of applying a second evaluation for identifying the problematic segments from the watershed segmentation, similar to our approach, by setting up a fixed set of rules on the segmented crowns. In this sense, a random sample consensus (RANSAC) was used by [57] to identify tree stems within detected tree clusters; those stems were then used as a starting point for clustering, by using normalised cut clustering to partition the points within a clump of trees into individual trees. The authors reported a detection rate less than 70%. On the other hand, reference [7] refined the first watershed delineations by further splitting the point cloud vertically, and then ran another set of watershed delineations over the lower layers by generating a multi-layered crown delineation. This notwithstanding, this approach was not suitable for tropical forests because the boundaries of the layers were fuzzy and difficult to identify [58].

The DBA algorithm improved the efficiency and accuracy of the tree attribute estimates and ITC detection and delineation [33]. However, while implementing DBA, generally, uncertainties in tree segmentations arose from the spacing threshold that we provide. In a sparse forest, the tree spacings are large and a relatively large threshold can be used to isolate the trees, but it is difficult to determine an appropriate threshold in a dense forest because a higher threshold can result in under-segmentation and a lower threshold can result in over-segmentation. This under and over-segmentation issue can be mitigated by using an adaptive threshold, assuming that taller trees are more widely spaced in the upper canopy level. Therefore, in our case, an adaptive spacing threshold was set to the DBA algorithm—to improve its efficiency in tree delineations—based on the knowledge we had of the respective forest study area and predetermined crown rules. We also incorporated additional classification rules (e.g., distance, distributions of points, and spatial structures) in the morphological opening procedures and semi-variogram statistics, which assisted us in determining a suitable range of crown sizes.

Since the generation of tree profiles relies on LiDAR point clouds, a high LiDAR point density is imperative for the accurate representation of tree profiles. If the LiDAR point density is relatively low (e.g., 1 point/m^2), a refinement of the method is needed to ensure that the proposed framework could still yield useful delineations. For future work, it would be interesting to determine the minimal LiDAR point densities that could be used for ITC delineation, to acquire LiDAR data more efficiently for operational consideration.

The accurate delineation of tree crowns plays a key role in estimating forest attributes at tree level and, subsequently, throughout the landscape. For instance, reference [17] reported that the average LiDAR-derived crown diameter explains 78% of the variance associated with biomass estimation. The increase in R^2 value was, on average, 0.11, with a maximum of 0.24, when 570 crown parameters were included. Without considering LiDAR-measured crown diameter variables, the RMSE value increased by up to 7 mg/ha. In our study, a simple assessment was made to determine how much AGB varies between single delineated trees (from the DBA results) and an overlapping crown of a misclassified tree (from the watershed segmentation results) (Figure 10). The AGB values from the DBA detected as two single trees were 1802.2 kg/tree and 2100 kg/tree, and the AGB value from the watershed that was detected as one tree was 2458.542 kg/tree. This is a huge difference in terms of AGB at the tree level—approximately 1443.7 kg/tree—which would possibly accumulate to a sizeable effect, if multiple mis-segmentations are present, at a landscape level.

Applications and prospective of LiDAR 3D point cloud-based ITC delineation procedures are numerous. The approach employed in this study allowed us to enhance the tree detection accuracy by 11%–16% compared to previous studies conducted in different forest environments. Even though ITC delineation is very computationally demanding, researchers should persist in the development of more accurate ITC delineations for several reasons. First, maps of trees have practical value for the

ecology and forestry sectors in South East Asia, especially in Malaysia. Ecologists, city planners and foresters need fine-scale maps to enforce zoning rules in riparian forests and understand the fate of trees within them [59–61]. Individual tree-based mapping can act as an excellent tool for this. Secondly, tracking the dynamics of the largest trees can account for a large carbon fraction in tropical forests that are especially vulnerable to drought, acting as an early warning signal to climate change [62,63]. Frequent LiDAR surveys could be valuable for this, but only the area-based approach has been used to date [63,64]. Additionally, the ITC approach may best match field-based techniques to measure forest carbon and has a strong theoretical basis in minimising bias and associated uncertainty [65].

5. Conclusions

By capitalizing on the usefulness of LiDAR data, a characterization of tree crown attributes was performed, and the accuracy of ITC delineation was improved using a new multi-step framework. Furthermore, the overall performance of the proposed method was validated at two forest sites to demonstrate its transferability to other forested areas with similar structural conditions. For each forest site, the proposed method detected individual tree crowns with a detection accuracy exceeding 80%. Our results showed high agreement ($R^2 > 0.64$) in terms of AGB estimates using 3D LiDAR metrics and variables measured in the field for both sites. The accuracy of LiDAR in retrieving tree crown height and CW at an individual-tree level using the framework presented was clearly demonstrated through a relative RMSE and bias less than 20%. Even though the desired accuracy of AGB was not fully attained, the framework presented significant improvements with respect to previous works. We hope that the promising results of ITC delineation and crown attribute estimation presented in this study will stimulate further research and applications in tropical forest sectors as well as other types of forest around the world.

Supplementary Materials: The following are available online at http://www.mdpi.com/1999-4907/9/12/759/s1, Table S1: Estimation results of tree height (CH), mean crown width (CW) and aboveground biomass (AGB) obtained from the ITCs delineated using watershed and DBA methods.

Author Contributions: W.S.W.M.J. collected and analyzed data, interpreted the results, prepared the manuscript, and coordinated revisions of the manuscript. I.H.W. supervised the work, assisted with the interpretation of the results and reviewed the manuscript versions. C.A.S. assisted in technical processing and the interpretation of the results and reviewed the manuscript versions. H.O. assisted in designing the fieldwork experiment and data collection strategies, provided access to a compilation of primary and secondary dataset, and reviewed the manuscript versions. K.N.A.M. provided comments and suggestions for revising the manuscript and identified potential sources for supporting this open access publication. A.T.H., M.M., A.C. and C.K. contributed to the interpretations and revisions of the manuscript. All authors have read and approved the final manuscript.

Funding: This work was supported by multiple sources, to which the authors are highly grateful: PhD scholarship from the MAJLIS AMANAH RAKYAT (MARA), Malaysia (Grant number: 330408224838), LAMB FUND, GEOGRAPHY CENTENARY, School of Geosciences, University of Edinburgh, UK (Fund code: E08802), ELIZABETH SINCLAIR IRVINE BEQUEST/CENTENARY AGROFORESTRY 89 FUND (Fund code: FPM 178413) and UKM-YSD Chair in Climate Change Fund from National University of Malaysia (UKM) (Grant number: ZF-2017-007).

Acknowledgments: Our utmost thanks to Forest Research Institute of Malaysia (FRIM) for providing an access to Pasoh Reserve Forest, sending their best field assistant to help in data collection and providing an access to the use of fieldwork instrument and their diligence with plot geolocation setup. We would also like to thank the survey team from the Faculty of Architecture, Planning and Surveying, MARA University of Technology, Malaysia for setting up a GPS plot location during the fieldwork campaign.

Conflicts of Interest: The authors declare no conflict of interest.

References

1. Lichstein, J.W.; Dushoff, J.; Ogle, K.; Chen, A.; Purves, D.W.; Caspersen, J.P.; Pacala, S.W. Unlocking the forest inventory data: Relating individual tree performance to unmeasured environmental factors. *Ecol. Appl.* **2010**, *20*, 684–699. [CrossRef] [PubMed]
2. Hyyppa, J.; Kelle, O.; Lehikoinen, M.; Inkinen, M. A segmentation-based method to retrieve volume estimates from 3-D tree height models produced by laser scanners. *IEEE Trans. Geosci. Remote Sens.* **2001**, *39*, 969–975. [CrossRef]
3. Krofcheck, D.J.; Litvak, M.E.; Lippitt, C.D.; Neuenschwander, A. Woody biomass estimation in a southwestern US juniper savanna using lidar-derived clumped tree segmentation and existing allometries. *Remote Sens.* **2016**, *8*, 453. [CrossRef]
4. Zhou, T.; Popescu, S.C.; Lawing, A.M.; Eriksson, M.; Strimbu, B.M.; Bürkner, P.C. Bayesian and classical machine learning methods: A comparison for tree species classification with LiDAR waveform signatures. *Remote Sens.* **2017**, *10*, 39. [CrossRef]
5. Vepakomma, U.; St-Onge, B.; Kneeshaw, D. Spatially explicit characterization of boreal forest gap dynamics using multi-temporal lidar data. *Remote Sens. Environ.* **2008**, *112*, 2326–2340. [CrossRef]
6. Hu, B.; Li, J.; Jing, L.; Judah, A. Improving the efficiency and accuracy of individual tree crown delineation from high-density LiDAR data. *Int. J. Appl. Earth Obs. Geoinf.* **2014**, *26*, 145–155. [CrossRef]
7. Duncanson, L.I.; Cook, B.D.; Hurtt, G.C.; Dubayah, R.O. An efficient, multi-layered crown delineation algorithm for mapping individual tree structure across multiple ecosystems. *Remote Sens. Environ.* **2014**, *154*, 378–386. [CrossRef]
8. Ferraz, A.; Saatchi, S.; Mallet, C.; Meyer, V. Lidar detection of individual tree size in tropical forests. *Remote Sens. Environ.* **2016**, *183*, 318–333. [CrossRef]
9. Lee, J.; Coomes, D.; Schonlieb, C.-B.; Cai, X.; Lellmann, J.; Dalponte, M.; Malhi, Y.; Butt, N.; Morecroft, M. A graph cut approach to 3D tree delineation, using integrated airborne LiDAR and hyperspectral imagery. *arXiv*, 2017; arXiv:1701.06715.
10. Wan-Mohd-Jaafar, W.S.; Woodhouse, I.; Silva, C.; Omar, H.; Hudak, A. Modelling individual tree aboveground biomass using discrete return LiDAR in lowland dipterocarp forest of Malaysia. *J. Trop. For. Sci.* **2017**, *29*, 465–484.
11. Hyyppa, J.; Hyyppa, H.; Leckie, D.; Gougeon, F.; Yu, X.; Maltamo, M. Review of methods of small-footprint airborne laser scanning for extracting forest inventory data in boreal forests. *Int. J. Remote Sens.* **2008**, *29*, 1339–1366. [CrossRef]
12. Lindberg, E.; Holmgren, J. Individual tree crown methods for 3D data from remote sensing. *Curr. For. Rep.* **2017**, *3*, 19–31. [CrossRef]
13. Chen, Q.; Baldocchi, D.; Gong, P.; Kelly, M. Isolating individual trees in a savanna woodland using small footprint lidar data. *Photogramm. Eng. Remote Sens.* **2006**, *72*, 923–932. [CrossRef]
14. Dalponte, M.; Ørka, H.O.; Ene, L.T.; Gobakken, T.; Næsset, E. Tree crown delineation and tree species classification in boreal forests using hyperspectral and ALS data. *Remote Sens. Environ.* **2014**, *140*, 306–317. [CrossRef]
15. Dalponte, M.; Reyes, F.; Kandare, K.; Gianelle, D. Delineation of individual tree crowns from ALS and hyperspectral data: A comparison among four methods. *Eur. J. Remote Sens.* **2015**, *48*, 365–382. [CrossRef]
16. Silva, C.A.; Hudak, A.T.; Vierling, L.A.; Loudermilk, E.L.; O'Brien, J.J.; Hiers, J.K.; Jack, S.B.; Gonzalez-Benecke, C.; Lee, H.; Falkowski, M.J.; et al. Imputation of individual longleaf pine (*Pinus palustris* Mill.) tree attributes from field and LiDAR data. *Can. J. Remote Sens.* **2016**, *42*, 554–573. [CrossRef]
17. Popescu, S.C.; Wynne, R.H.; Nelson, R.F. Measuring individual tree crown diameter with lidar and assessing its influence on estimating forest volume and biomass. *Can. J. Remote Sens.* **2003**, *29*, 564–577. [CrossRef]
18. Tiede, D.; Hochleitner, G.; Blaschke, T. A full GIS-based workflow for tree identification and tree crown delineation using laser scanning. *ISPRS Workshop CMRT* **2005**, *5*, 9–14.
19. Zhen, Z.; Quackenbush, L.J.; Zhang, L.J. Impact of tree-oriented growth order in marker-controlled region growing for individual tree crown delineation using airborne laser scanner (ALS) data. *Remote Sens.* **2014**, *6*, 555–579. [CrossRef]
20. Koch, B.; Heyder, U.; Weinacker, H. Detection of individual tree crowns in airborne lidar data. *Photogramm. Eng. Remote Sens.* **2006**, *72*, 357–363. [CrossRef]

21. Brandtberg, T. Individual tree-based species classification in high spatial resolution aerial images of forests using fuzzy sets. *Fuzzy Sets Syst.* **2002**, *132*, 371–387. [CrossRef]
22. Liu, Q.; Jing, L.; Li, Y.; Tang, Y.; Li, H.; Lin, Q. *A Tree Canopy Height Delineation Method Based on Morphological Reconstruction—Open Crown Decomposition*; IOP Conference Series: Earth and Environmental Science; IOP Publishing: Halifax, NS, Canada, 2016; pp. 12–20.
23. Wang, L. A multi-scale approach for delineating individual tree crowns with very high resolution imagery. *Photogramm. Eng. Remote Sens.* **2010**, *76*, 371–378. [CrossRef]
24. Jing, L.H.; Hu, B.X.; Noland, T.; Li, J.L. An individual tree crown delineation method based on multi-scale segmentation of imagery. *ISPRS J. Photogramm. Remote Sens.* **2012**, *70*, 88–98. [CrossRef]
25. Falkowski, M.J.; Smith, A.M.S.; Hudak, A.T.; Gessler, P.E.; Vierling, L.A.; Crookston, N.L. Automated estimation of individual conifer tree height and crown diameter via two-dimensional spatial wavelet analysis of lidar data. *Can. J. Remote Sens.* **2006**, *32*, 153–161. [CrossRef]
26. Wolf, B.M.; Heipke, C. Automatic extraction and delineation of single trees from remote sensing data. *Mach. Vis. Appl.* **2007**, *18*, 317–330. [CrossRef]
27. Holmgren, J.; Barth, A.; Larsson, H.; Olsson, H. Prediction of stem attributes by combining airborne laser scanning and measurements from harvesters. *Silva Fenn.* **2012**, *46*, 227–239. [CrossRef]
28. Vauhkonen, J.; Korpela, I.; Maltamo, M.; Tokola, T. Imputation of single-tree attributes using airborne laser scanning-based height, intensity, and alpha shape metrics. *Remote Sens. Environ.* **2010**, *114*, 1263–1276. [CrossRef]
29. Lloyd, S. Least squares quantization in PCM. *IEEE Trans. Inf. Theor.* **1982**, *28*, 129–137. [CrossRef]
30. Morsdorf, F.; Meier, E.; Allgöwer, B.; Nüesch, D. Clustering in airborne laser scanning raw data for segmentation of single trees. *Int. Arch. Photogramm. Remote Sens. Spat. Inf. Sci.* **2003**, *34*, W13.
31. Gupta, S.; Weinacker, H.; Koch, B. Comparative analysis of clustering-based approaches for 3-D single tree detection using airborne fullwave lidar data. *Remote Sens.* **2010**, *2*, 968–989. [CrossRef]
32. Lee, H.; Slatton, K.C.; Roth, B.; Cropper Jr, W. Adaptive clustering of airborne LiDAR data to segment individual tree crowns in managed pine forests. *Int. J. Remote Sens.* **2010**, *31*, 117–139. [CrossRef]
33. Li, W.K.; Guo, Q.H.; Jakubowski, M.K.; Kelly, M. A new method for segmenting individual trees from the lidar point cloud. *Photogramm. Eng. Remote Sens.* **2012**, *78*, 75–84. [CrossRef]
34. Ferraz, A.; Bretar, F.; Jacquemoud, S.; Gonçalves, G.; Pereira, L. 3D Segmentation of Forest Structure Using a Mean-Shift Based Algorithm, Image Processing (ICIP). In Proceedings of the 17th IEEE International Conference, Hong Kong, China, 22–26 March 2010; pp. 1413–1416.
35. Ferraz, A.; Bretar, F.; Jacquemoud, S.; Goncalves, G.; Pereira, L.; Tome, M.; Soares, P. 3-D mapping of a multi-layered Mediterranean forest using ALS data. *Remote Sens. Environ.* **2012**, *121*, 210–223. [CrossRef]
36. Hu, X.; Xie, Y. Segmentation and Clustering of 3D Forest Point Cloud Using Mean Shift Algorithms. In Proceedings of the 4th International Conference on Machinery, Materials and Computing Technology (ICMMCT 2016), Hangzhou, China, 23–24 January 2016; 2016; pp. 1275–1279.
37. Amiri, N.; Yao, W.; Heurich, M.; Krzystek, P.; Skidmore, A.K. Estimation of regeneration coverage in a temperate forest by 3D segmentation using airborne laser scanning data. *Int. J. Appl. Earth Obs. Geoinf.* **2016**, *52*, 252–262. [CrossRef]
38. Comaniciu, D.; Meer, P. Mean shift: A robust approach toward feature space analysis. *IEEE Trans. Pattern Anal. Mach. Intell.* **2002**, *24*, 603–619. [CrossRef]
39. Ahmad Fitri, Z.; Nizam, M.S.; Latiff, A.; Nur Supardi, M.N.; Abd Rahman, K.; Christine, D.F. Distribution analysis and productivity of Myristicaceae in 50-ha plot at Pasoh Forest Reserve, Negeri Sembilan, Malaysia. *Malays. For.* **2018**, *81*, 11–33.
40. Nazre, M.; Nazariah, N.; Mat-Salleh, K.; Latiff, A.; Faridah Hanum, I. Dynamics and Spatial Distribution of Garcinia in Pasoh Forest Reserve, Negeri Sembilan, Malaysia. In Proceedings of the Symposium and Workshop of Forest-People in the Humid Tropics: Past, Present and Future Hydrological Research for Integrated Land and Water Management, Hotel Equatorial Bangi, Malaysia, 30 July–4 August 2000.
41. McGaughey, R.J. Fusion/LDV: Software for LiDAR Data Analysis and Visualization Version 3.50. Available online: http://forsys.cfr.washington.edu/fusion/FUSION_manual.pdf (accessed on 15 June 2015).
42. Soille, P. Morphological phase unwrapping. *Opt. Laser Eng.* **1999**, *32*, 339–352. [CrossRef]
43. Clark, I. Geostatistics. 2. Semivariogram. 1. *Eng. Min. J.* **1979**, *180*, 90–94.

44. St-Onge, B.; Cavayas, F. Estimating forest stand structure from high resolution imagery using the directional variogram. *Int. J. Remote Sens.* **1995**, *16*, 1999–2021. [CrossRef]
45. Meyer, F.; Beucher, S. Morphological segmentation. *J. Vis. Commun. Image Represent.* **1990**, *1*, 21–46. [CrossRef]
46. Vincent, L.; Soille, P. Watersheds in digital spaces: An efficient algorithm based on immersion simulations. *IEEE Trans. Pattern Anal. Mach. Intell.* **1991**, *6*, 583–598. [CrossRef]
47. Brandtberg, T.; Warner, T.A.; Landenberger, R.E.; McGraw, J.B. Detection and analysis of individual leaf-off tree crowns in small footprint, high sampling density lidar data from the eastern deciduous forest in North America. *Remote Sens. Environ.* **2003**, *85*, 290–303. [CrossRef]
48. Hadji, I.; Nabelek, D. Clustering algorithms used in 3D scene segmentation. Available online: http://vigir.missouri.edu/~{}hadjisma/links/project2_Final.pdf (accessed on 9 August 2018).
49. *R: A Language and Environment for Statistical Computing*; Team, R.D.C.: Vienna, Austria, 2016.
50. Goutte, C.; Gaussier, E. A Probabilistic Interpretation of Precision, Recall and F-score, with Implication for Evaluation. In Proceedings of the European Conference on Information Retrieval, Santiago de Compostela, Spain, 21–23 March 2005; pp. 345–359.
51. Sokolova, M.; Japkowicz, N.; Szpakowicz, S. Beyond Accuracy, F-score and ROC: A Family of Discriminant Measures for Performance Evaluation. In *Proceedings of the Australasian Joint Conference on Artificial Intelligence*; Springer: Hobart, Australia, 2006; pp. 1015–1021.
52. Hollander, M.; Wolfe, D.A. *Nonparametric Statistical Methods*, 2nd ed.; John Wiley & Sons: New York, NY, USA, 1999; p. 787.
53. Silva, C.A.; Crookston, N.L.; Hudak, A.T.; Vierling, L.A. rLiDAR: An R Package for Reading, Processing and Visualizing LiDAR (Light Detection and Ranging) Data, Version 0.1. Available online: https://cran.r-project.org/web/packages/rLiDAR/index.html (accessed on 19 May 2015).
54. Silva, C.; Klauberg, C.; Hudak, A.; Vierling, L.; Jaafar, W.; Mohan, M.; Saatchi, S. Predicting stem total and assortment volumes in an industrial pinus taeda L. Forest plantation using airborne laser scanning data and random forest. *Forests* **2017**, *8*, 254. [CrossRef]
55. Jakubowski, M.K.; Li, W.; Guo, Q.; Kelly, M. Delineating individual trees from LiDAR data: A comparison of vector-and raster-based segmentation approaches. *Remote Sens.* **2013**, *5*, 4163–4186. [CrossRef]
56. Mohan, M.; Silva, C.A.; Klauberg, C.; Jat, P.; Catts, G.; Cardil, A.; Dia, M. Individual tree detection from unmanned aerial vehicle (UAV) derived canopy height model in an open canopy mixed conifer forest. *Forests* **2017**, *8*, 340. [CrossRef]
57. Reitberger, J.; Schnorr, C.; Krzystek, P.; Stilla, U. 3D segmentation of single trees exploiting full waveform LIDAR data. *ISPRS J. Photogramm. Remote Sens.* **2009**, *64*, 561–574. [CrossRef]
58. Kwak, D.A.; Lee, W.K.; Lee, J.H.; Biging, G.S.; Gong, P. Detection of individual trees and estimation of tree height using LiDAR data. *J. For. Res.* **2007**, *12*, 425–434. [CrossRef]
59. Huo, L.Z.; Silva, C.A.; Klauberg, C.; Mohan, M.; Zhao, L.J.; Tang, P.; Hudak, A.T. Supervised spatial classification of multispectral LiDAR data in urban areas. *PLoS ONE* **2018**, *13*, e0206185. [CrossRef] [PubMed]
60. Zhao, F.; Guo, Q.; Kelly, M. Allometric equation choice impacts lidar-based forest biomass estimates: A case study from the Sierra National Forest, CA. *Agric. For. Meteorol.* **2012**, *165*, 64–72. [CrossRef]
61. Mohamad-Roslan, M.K.; Shamsul, K. Characterization of riparian plant community in lowland forest of peninsular Malaysia. *Int. J. Bot.* **2012**, *8*, 181–191.
62. Jaskierniak, D.; Lane, P.N.; Robinson, A.; Lucieer, A. Extracting LiDAR indices to characterise multilayered forest structure using mixture distribution functions. *Remote Sens. Environ.* **2011**, *115*, 573–585. [CrossRef]
63. Simonson, W.; Ruiz-Benito, P.; Valladares, F.; Coomes, D. Modelling above-ground carbon dynamics using multi-temporal airborne lidar: Insights from a Mediterranean woodland. *Biogeosciences* **2016**, *13*, 961–973. [CrossRef]

64. Roise, J.P.; Harnish, K.; Mohan, M.; Scolforo, H.; Chung, J.; Kanieski, B.; Shen, T. Valuation and production possibilities on a working forest using multi-objective programming, Woodstock, timber NPV, and carbon storage and sequestration. *Scand. J. For. Res.* **2016**, *31*, 674–680. [CrossRef]
65. Coomes, D.A.; Dalponte, M.; Jucker, T.; Asner, G.; Banin, L.F.; Burslem, D.F.; Lewis, S.L.; Nilus, R.; Phillips, O.L.; Phua, M.H.; et al. Area-based vs tree-centric approaches to mapping forest carbon in Southeast Asian forests from airborne laser scanning data. *Remote Sens. Environ.* **2017**, *194*, 77–88. [CrossRef]

© 2018 by the authors. Licensee MDPI, Basel, Switzerland. This article is an open access article distributed under the terms and conditions of the Creative Commons Attribution (CC BY) license (http://creativecommons.org/licenses/by/4.0/).